Polarization Lidar and Synoptic Analyses of an Unusual Volcanic Aerosol Cloud

KENNETH SASSEN AND JOHN D. HOREL

Department of Meteorology, University of Utah, Salt Lake City, Utah

(Manuscript received 8 February 1990, in final form 29 May 1990)

ABSTRACT

Over an unusually brief three-day period in early August 1989, spectacular twilight effects indicative of a stratospheric volcanic cloud were seen at Salt Lake City, Utah. Concurrent polarization lidar observations detected an aerosol layer at altitudes between 14 and 16 km in the vicinity of the tropopause. Trajectory analyses indicate that the aerosol source was the relatively minor 19 July volcanic eruption of Santiaguito in Guatemala. Materials injected into the lower stratosphere by this eruption were transported initially by tropical easterlies and then by a subtropical jet stream to the locale. The sulfuric acid droplet cloud that formed during transport was affected locally by tropopause folds that promoted stratospheric–tropospheric exchanges. Although lidar depolarization analysis suggests that the ensuing cloud microphysical processes were usually dominated by acid droplet crystallization effects caused by ammonia gas absorption (yielding 0.1–0.2 linear depolarization ratios), there is also evidence for ice crystals at the coldest temperatures (~ -64°C) and for homogeneous droplets. Cloud optical thickness estimates are 0.01–0.02. Mesoscale cloud bands were observed visually near sunset and also occasionally during daylight, another unusual characteristic for volcanic clouds.

1. Introduction

Atmospheric effects resulting from volcanic eruptions vary considerably in magnitude due to several factors. Major explosive eruptions capable of causing global effects and recognizable climatic perturbations appear to be rare and occur, perhaps, only a few times per century (Self et al. 1981). The eruption of the Mexican volcano El Chichón during March and April 1982 provided a textbook example of a volcanically injected stratospheric aerosol cloud that was linked to possible climatic perturbations (for a recent review, see Ardanuy and Kyle 1986). Typically it is not the ash component of the eruption cloud, which tends to settle out comparatively quickly, but the makeup of the gaseous effluent that determines the eventual mass loading and persistence of the aerosol cloud (Rampino and Self 1984). The relatively minor October 1974 eruption of Valcán de Fuego in Guatemala, for example, produced a long-lived stratospheric aerosol cloud (McCormick et al. 1978) because of its sulfur-enriched gas injections. The height attained by the eruption cloud is also of considerable importance since the plume must penetrate far enough into the stratosphere to promote aerosol formation and delay the eventual removal of the debris through sedimentation and tropospheric mixing. Even the season and latitude of the eruption affect the change in the planet's radiation budget as a function of the rate; the aerosols are redistributed latitudinally before the cloud decays.

The evolution and composition of the aerosol cloud that formed from the El Chichón emissions was studied in some detail with modern research instrumentation. The eruptions initially injected sulfurous gases, mainly SO_2, and particulates up to a height of $\sim$26 km. Subsequent photooxidation and gas-phase chemical reactions led to the production of sulfate species and, most importantly, to sulfuric acid vapor that rapidly condensed into H_2SO_4/H_2O droplets. In situ particle measurements revealed a bimodal sulfuric acid droplet size distribution with maximum radii of 0.02 and 0.7 μm reflecting both continuing new nucleation and droplet vapor growth and coalescence (Hofmann and Rosen 1983). These processes continued for several months over an expanding area that eventually covered the globe. (In the three weeks following the eruption the aerosols rapidly propagated westward forming a well-defined zonal band.) The migration of the aerosol into the polar regions of both hemispheres was studied by aircraft remote sensing and satellite observations, which revealed rather significant (and poorly understood) spatial and temporal variations in the optical properties of the spreading cloud (e.g., see McCormick and Swissler 1983).

In this article, we describe a relatively brief occurrence of what was undoubtedly an aerosol cloud of volcanic origin on the basis of ground-based polarization lidar measurements collected from 4 to 7 August 1989 at the Facility for Atmospheric Remote Sensing (FARS) in Salt Lake City, Utah (40.8°N, 111.8°W).

Corresponding author address: Prof. Kenneth Sassen, University of Utah, Department of Meteorology, 819 Wm. C. Browning Bldg., Salt Lake City, Utah 84112.

Although the lidar system was designed for tropospheric cloud studies, these observations were initiated in response to rather spectacular red sunsets indicating an elevated layer that could be detected by our system. Occasionally, barely discernable cloud bands were also visible during daylight. The ruby lidar detected a scattering layer between 14 and 16 km (all heights are given above mean sea level) whose peak backscattering level gradually rose over three successive evenings. As will be shown here, the laser depolarization produced by the aerosols appears to be consistent with sulfur-based compounds of volcanic origin.

The apparent absence of any recent major volcanic activity and the uncharacteristically brief appearance of this relatively dense material prompted us to perform preliminary trajectory analyses. It was immediately apparent that the transport of the aerosol was associated with a subtropical jet stream with the aerosols originating several days before from the central Pacific region and, before that, from Central America. It follows that this unusual occurrence of a "mystery" cloud provides insights into (1) a transport mechanism responsible for the latitudinal spreading and the tropospheric subduction of lower stratospheric aerosols, and (2) the evolving microphysical processes occurring in a volcanic aerosol layer that was modified by stratospheric–tropospheric exchanges within a tropopause fold.

At this time, however, we are not without a promising candidate volcano to account for the observations. On 19 July 1989, or about two weeks prior to the first Salt Lake City observations, the volcanic dome, Santiaguito (14.8°N, 91.6°W), erupted in Guatemala. A dense ash cloud was injected up to an altitude of ~6.5 km, and higher eruption clouds were also noted (SEAN Bulletin 1989). The dynamics of the eruption cloud are still under investigation, but, as shown here, this volcano is a probable source for the aerosols, assuming that sufficient sulfurous gases were injected into the lower stratosphere. (Although the Santiaguito, El Chichón, and Fuego volcanoes are located in the same general region, Santiaguito has not previously been known as a comparable producer of SO_2 because of differences in the magma type.)

2. Aerosol transport in the lower stratosphere

Conventional synoptic data and gridded analyses from the numerical models of the National Meteorological Center are received in near real time at the University of Utah (Horel et al. 1988). Here, the gridded data on standard pressure levels between 1000 and 100 mb are linearly interpolated to isentropic surfaces in a manner similar to that of Crum and Stevens (1988). In view of lidar evidence indicating the local presence of aerosols between ~110 and 150 mb, available synoptic data from the 100 mb level and below are used in this study to approximate the lower stratospheric circulation associated with the aerosol transport.

The vector wind field and Montgomery streamfunction on the 375 K surface, the highest level that remained at or below 100 mb over the domain, are shown in Fig. 1 for 0000 UTC (all times are UTC) 20 July, roughly 9-h after the Santiaguito eruption. On the basis of this wind field, any aerosols injected into the lower stratosphere by Santiaguito (14.8°N, 91.6°W) would be carried initially towards the south and southwest. The large-scale circulation in the lower stratosphere is characterized by easterly winds extending from Central America towards Hawaii and by southwesterly winds extending from Hawaii towards the United States. The principal features of the circulation generally remained stationary during the following three weeks, and trajectory analyses show favorable conditions for the advection of Santiaguito materials to the Salt Lake City (SLC) area at about the time they were observed locally.

In order to estimate the path taken by aerosols possibly produced by Santiaguito, trajectories on isentropic surfaces are computed using the trajectory analysis scheme of Crum and Stevens (1988). Figure 2 illustrates a trajectory on the 375 K surface that starts at 0000 20 July in the vicinity of Santiaguito and travels to near SLC by 0000 4 August or shortly before the aerosol cloud was observed there. The parcel initially travels westward and reaches 10°N, 140°W by 0000 28 July. Afterwards, the parcel begins to move northward and is entrained into the southwesterly flow that is evident in Fig. 1. The strong southwesterly flow rapidly carries the parcel across the United States during the 3–5 August period. Along its trajectory, the parcel descends from 110 to 144 mb near SLC.

In general, the location of the entrainment of tropical air into the southwesterly flow extending into the western United States strongly affects the path of the trajectories. As a result of the presence of an upper tropospheric–lower stratospheric trough to the east of Hawaii during the 28 July to 1 August period, trajectories that arrive in the vicinity of Hawaii are most likely to be carried toward North America. However, it should be remarked that the uncertainties introduced by this type of trajectory scheme can contribute errors to each parcel's path, and it should be viewed as somewhat fortuitous that the trajectory in Fig. 2 passes so close to SLC.

Focusing attention on the lower stratospheric circulation in the vicinity of SLC during the period of interest, the predominant synoptic scale factors in the upper troposphere and lower stratosphere were: 1) the broad southwesterly flow that is evident in Fig. 1 with the main jet axis to the south (north) of SLC prior to (after) 5 August, and 2) jet streaks embedded within this current that remained ill-defined by conventional synoptic data. Time height sections of wind speed, temperature, and potential temperature derived from 12-hourly SLC radiosonde observations are shown in Fig. 3 for the 1–8 August period. Two jet maxima, one

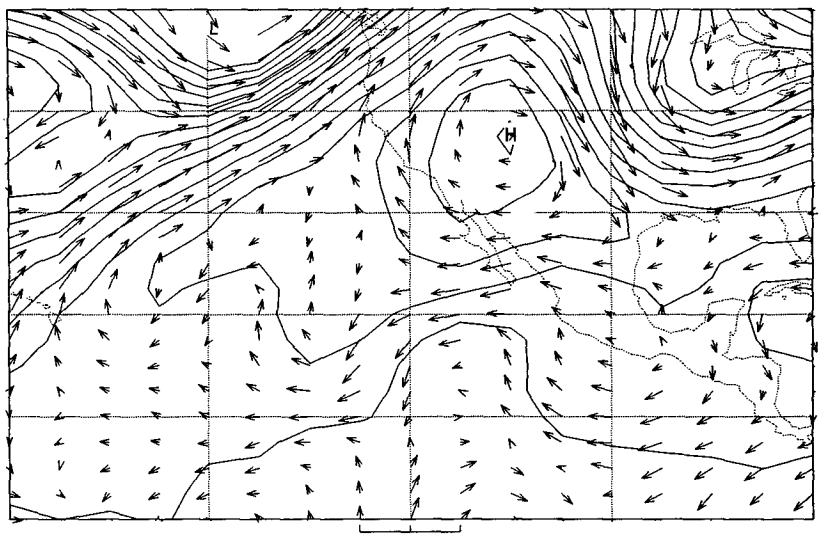

FIG. 1. 373 K Montgomery stream function and wind field from the MRF model for 0000 UTC 20 July 1989. The contour interval is 250 $m^2 s^{-2}$ and the wind speed scale is shown at bottom (full scale is 50 m s^{-1}).

between 0000 and 1200 UTC 3 August and another stronger jet between 0000 and 1200 UTC 5 August, are evident. The passage of the jet streak on 5 August is clearly present in the time-height sections of temperature (Fig. 3b) and potential temperature (Fig. 3c). Cross sections (not shown) oriented perpendicular to this jet streak show a well-defined upper-level frontal structure and the potential for strong stratospheric–tropospheric exchange.

Superimposed on each panel of Fig. 3 are the heights of the cloud layer (the bars) as measured by lidar from 4 to 7 August. The aerosols were found between about 14 and 16 km, where temperatures ranged from −55° to −65°C and potential temperatures from 370 to 400 K. From 4 to 6 August, the aerosol layer lifts slightly, which may be due to large-scale ridging over the western United States (note the slight rising trend of the 375 K surface from 3 to 7 August in Fig. 3). Although the isentropic surfaces in the lower stratosphere dropped sharply with the passage of the jet streak and associated tropopause fold at 0000 UTC 5 August, the height of the aerosol layer appears insensitive to its passage. The reasons for this remain unclear, but Post (1986) has suggested that the heights of decaying volcanic debris are influenced by the advection of materials affected by upwind jet streak activity. It can be deduced that the aerosols likely experienced synoptic-scale vertical motions on the order of ±1 to 3 cm s^{-1} and, in the vicinity of the embedded jet streaks, stronger motions on the order of ±5 cm s^{-1} (Keyser and Shapiro 1986).

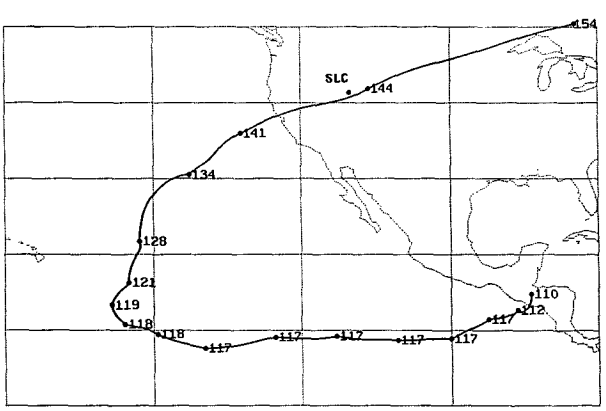

FIG. 2. A trajectory on the 375 K surface (computed using a 15 min time step) that starts in the vicinity of Santiaguito on 0000 UTC 20 July and continues until 0000 UTC 5 August. Dots indicate the location of the parcel at 1 day intervals, and the parcel's pressure at those times is also shown.

3. Polarization lidar observations

a. Data collection and analysis

The FARS lidar employs a relatively high power (1.5 J) but low PRF (effectively 2 shots min^{-1}) ruby laser system with a 0.694 μm wavelength. Data acquisition of the two polarization channels is accomplished simultaneously at 7.5 m spatial resolution and with a maximum range of 14.6 km above ground level (16.1 km MSL). (A few profiles on each day were obtained at 15 m resolution, extending the maximum range to ~30 km.) Data processing to obtain volume backscatter coefficients, as described recently in Sassen et al. (1989a), is normally based on a "clear air" calibration that provides a boundary condition (i.e., mo-

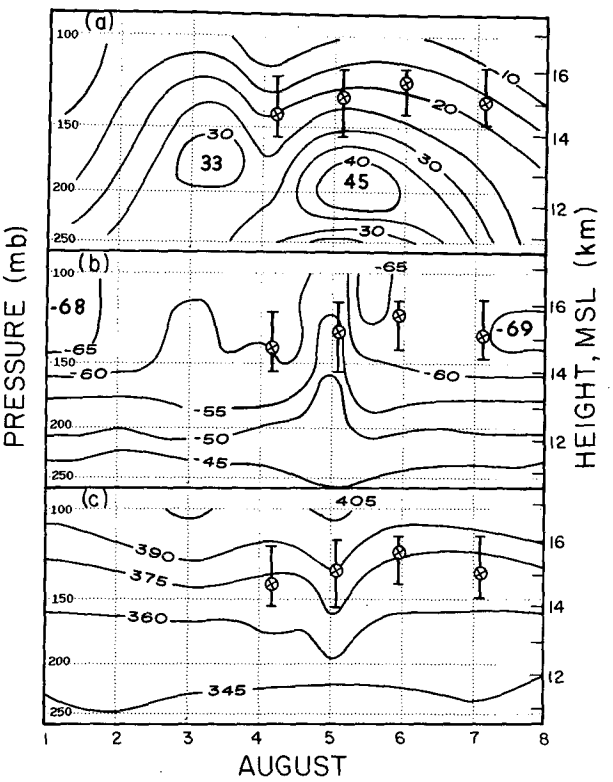

FIG. 3. Height-time cross sections between 250–100 mb for (a) wind speed (contoured in 5 m s^{-1} intervals), (b) temperature (5°C intervals), and (c) potential temperature (15 K intervals) for the period of 1 to 8 August, derived from Salt Lake City radiosonde data. In all panels the lidar-measured cloud thicknesses and peak scattering heights are shown by vertical bars and "×" symbols, respectively.

lecular backscattering as a function of air density obtained from concurrent radiosonde data) to solve the lidar equation. In this case, however, it was found necessary to apply an aerosol correction factor to the "molecular" signals below the well-defined cloud layers (see McCormick et al. 1978) in order to generate stable lidar equation solutions. The data quantities derived from the lidar signal analysis include the scattering ratio,

$$R(z) = \frac{\beta_t(z)}{\beta_m(z)}, \tag{1}$$

and the cloud optical thickness,

$$\tau_c = \frac{1}{k}\int_{z_b}^{z_t} \beta_c(z)dz, \tag{2}$$

where β is the volume backscatter coefficient (km^{-1} sr^{-1}) with subscripts m, c, and t referring to the molecular, cloud, and total ($m + c$) components; k is the backscatter-to-extinction coefficient ratio (sr^{-1}) and z is height.

In deriving τ_c the cloud backscatter coefficient is integrated vertically between the cloud base z_b and top z_t heights and an appropriate value of k (taken as a constant for numerical simplicity) must be specified. Assuming that the aerosol is composed of droplets of 75% H_2SO_4 in aqueous solution (see Russell and Hadke 1977), Fig. 4 shows Mie theory scattering predictions of k for three zeroth-order logarithmic distributions at the ruby laser wavelength. The three standard deviations encompass a fairly wide range of size distributions for droplet modal radii r_m in the 0.01–1.5 μm range representative of stratospheric aerosols. The selection of k obviously depends on knowledge of r_m, but the range of possibilities is not extreme in this case.

Finally, linear depolarization ratios (δ values) are derived from the ratio of the perpendicular-to-parallel polarized returned laser powers without attempting to adjust for molecular and background aerosol scattering (see Kobayashi et al. 1987). Since laser depolarization is sensitive to the shape of cloud particles, this technique is a powerful tool for inferring cloud composition. Recently, Sassen et al. (1989b) reviewed the evidence obtained from polarization lidar studies of stratospheric clouds and provided new laboratory data on the laser scattering properties of evaporating sulfuric acid droplets undergoing crystallization from reaction product formation due to ammonia gas absorption. In summary, δ values of 0.10–0.15 were measured for clouds composed of partially crystallized H_2SO_4 droplets, which contrast with the $\delta \approx 0.01$ (or slightly higher in the presence of multiple scattering) for optically homogeneous acid droplets and the $\delta \approx 0.5$ for stratospheric ice crystals nucleated (presumably) through the homogeneous freezing of diluted solution droplets.

Lidar observations were obtained at 0.5 or 1.0 min intervals over the following time periods: 0311–0500

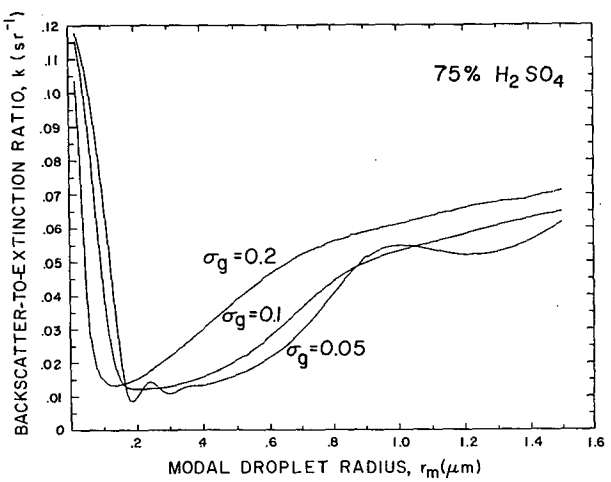

FIG. 4. Mie scattering theory predictions for the backscatter-to-extinction ratio k as a function of modal droplet radius for logarithmic size distributions with the three indicated standard deviations σ_g. Computations are based on a refractive index appropriate for 75% sulfuric acid solution droplets. The variations in the $\sigma_g = 0.05$ curve represent scattering resonances that are apparent because of the narrowness of the size distribution.

4 August; 0218–0404 and 2224–2330 5 August; and 0243–0259 7 August. However, only a limited number of profiles from the aerosol region were obtained on 5 August due to the interference caused by tropospheric clouds, and only very weakly scattering residual aerosols were detected on 7 August. The data have been treated to minimize the effects of signal noise by performing averaging techniques that are sufficient to provide the best possible spatial and temporal resolutions and also to provide the most reliable data on bulk cloud properties.

b. *Cloud layer structure*

Unlike the uniform twilight effects typically seen following major volcanic eruptions, a considerable amount of cloud structure was observed visually in the reddened sunset sky. Although these effects show up more vividly in color photography, Fig. 5 provides a black and white image, taken just before sunset on 5 August, of cloud bands made visible by solar forward scattering. Both mesoscale cloud bands and embedded gravity wave patterns were observed. Figure 6a–b illustrates the temporal changes in the internal structure of the cloud layers derived from the ~2-h data records collected on 4 and 5 August, which likely correspond to the observed mesoscale cloud bands.

This figure shows height-versus-time (HTI) displays of the scattering ratio R and the linear depolarization ratio δ. The original dataset was examined to remove profiles affected by tropospheric cloud blockage, and averages of ten profiles consisting of 75-m (10-point) vertical averages were used to reduce the effects of signal noise and (8-bit) data digitizer errors. The scattering ratio contours for both periods reveal a horizontally stratified layer that contains wave-like concentrations of scattering material. The layer containing the peak 6.0–8.0 scattering ratios rises from near cloud base to near cloud top over the 24-h period. The depolarization data indicate a surprising amount of variability in the microphysical composition of the clouds. Although $\delta \approx 0.15$ are most common, individual δ averages vary from 0.01 to 0.45, and 0.01 to 0.24 on 4 and 5 August, respectively. The depolarization fields also display mesoscale variations in association with the scattering ratio patterns. Particularly interesting is the lens of relatively high δ values near cloud top at ~0415 4 August. The δ values suggest the presence of ice crystals at the coldest temperatures (~ −64°C) in the vicinity of the tropopause. These high depolarizations occur above a region containing the highest observed scattering ratios and seem to define the cap of a mesoscale wave structure, whereas the pattern in the δ value contours suggests ice crystal precipitation from the near cloud-top generating region. During both observation periods, the strongest backscattering regions tend to display $\delta \approx 0.1$–0.2, perhaps an indication that relatively large partially-crystallized droplets were present in those regions.

c. *Average cloud properties*

Normally, due to the high altitudes and weak backscattering typical of stratospheric aerosols, considerable lidar signal integration (often over a few hours) is performed to recover reliable data quantities. In order to allow intercomparisons with the mean properties of stratospheric aerosol layers reported elsewhere, data

FIG. 5. Wide-angle photograph of the structure observed in the volcanic cloud layer at 0220 5 August, just before sunset.

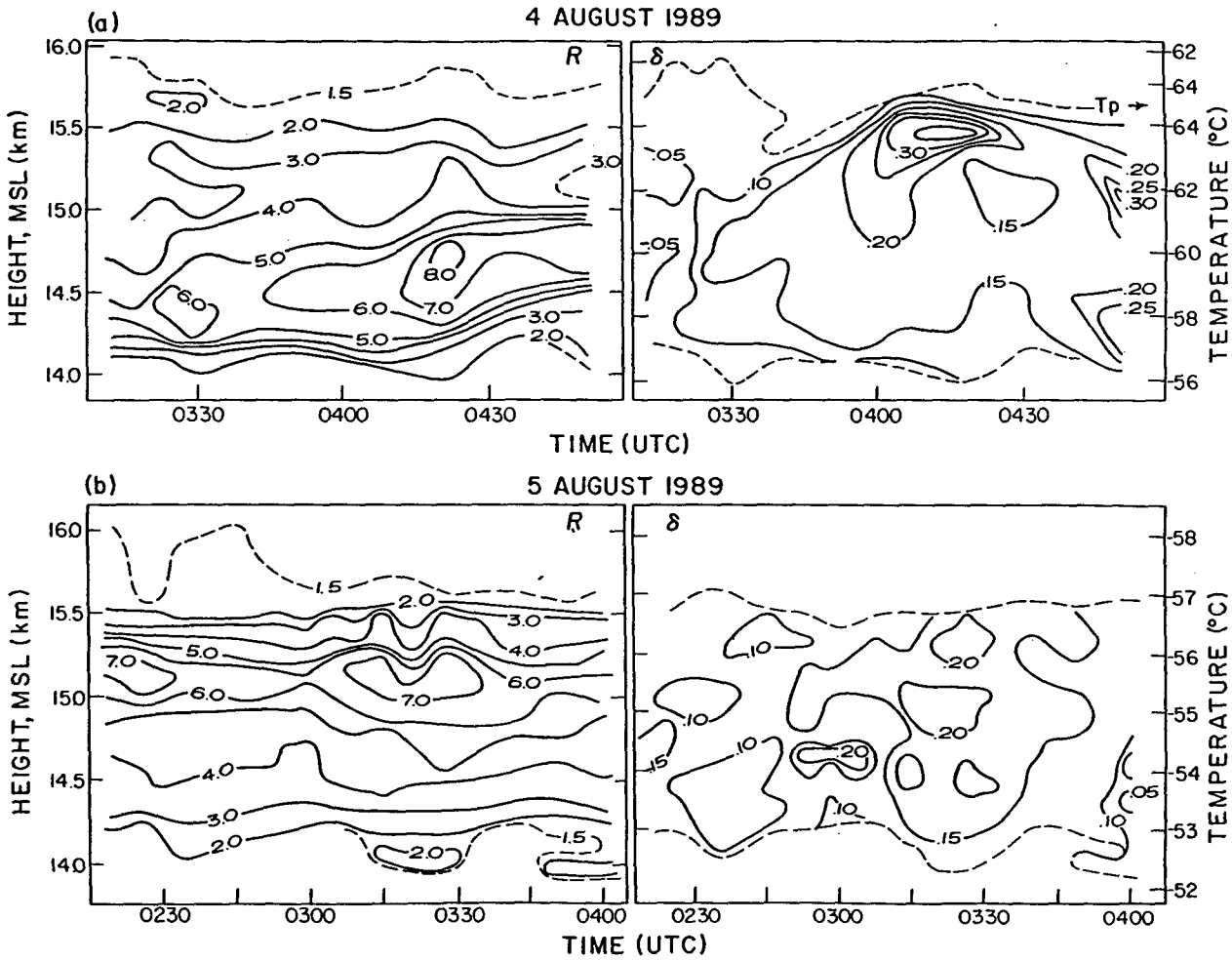

FIG. 6. Height-versus-time lidar displays of averaged scattering ratio R (left of each pair) and linear depolarization ratio δ for a) 4 August and b) 5 August, illustrating the mesoscale cloud structure shown in the photograph of Fig. 5. Temperature scales are based on the closest SLC radiosonde profiles, where T_p refers to the tropopause height. Note that at 0000 UTC 5 August, T_p = 11.3 km as a result of the folded tropopause over SLC.

quantities representing the average of all lidar profiles collected during the four observation periods are given in Fig. 7a–d. Table 1 summarizes these findings.

The scattering ratio profiles in Fig. 7 clearly show the gradual ascent, at a rate of ~0.6 km day^{-1}, and strengthening of the cloud layer peak. By 7 August, only a residual aerosol layer between ~14.0–16.0 km was observed in the lower stratosphere. Optical thickness estimates, based on the use of an average backscatter-to-extinction ratio of k = 0.04 appropriate for small sulfuric acid droplets (see Fig. 4), are given in Table 1. The average and 10-shot maximum τ_c of about 0.01–0.02 are slightly below the ~0.03 threshold for the visual detection of cirrus clouds reported by Sassen et al. (1989a). Since waves in the cloud layer were seen near the zenith on a few occasions during the day on 4 and 5 August, these clouds could have a similar subvisual-versus-visible τ_c threshold. The aerosols observed on 7 August, which produced only a slight reddening of the sunset sky, yielded an estimated optical thickness of 0.0015.

The linear depolarization ratios derived from the averaged returns (the dashed lines in Fig. 7) show that the integrated values are typically around 0.15. This amount of depolarization is consistent with laboratory experiments of crystallized sulfuric acid droplets, although it should be recalled that Fig. 6 reveals smaller scale variations over the 0.01 to 0.45 range indicative of homogeneous droplets and ice crystals, respectively. Quite low δ values are associated with the strong cloud peak on 5 August (Fig. 7c), also indicating spherical, homogeneous scatterers. To help evaluate the cause of the δ value variability, a scatter plot of all 10-shot 75 m height averages collected during the four observation periods is given in Fig. 8. The weak aerosol data obtained on 7 August, shown by the "●" points, display considerably less scatter than the cloud values shown by the "×" symbols. The scatter that is present in the

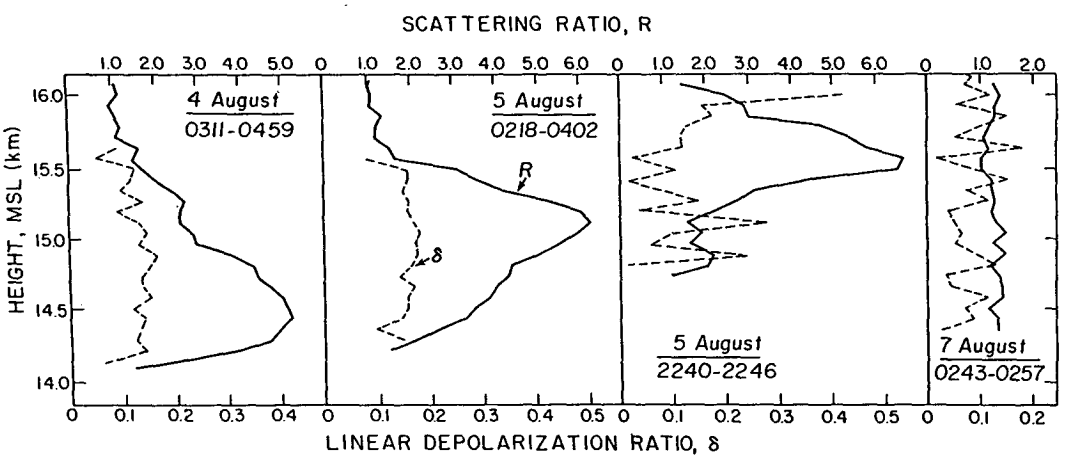

FIG. 7. Profiles of scattering ratio R (solid) and linear depolarization ratio δ (dashed) derived from the average of all lidar shots collected during the four indicated observation periods. The δ values derived from the short data segments in the right two panels illustrate the effects of signal noise.

aerosol data is largely a consequence of noise effects in weak signals, since longer averages mainly produce 0.05–0.10 δ values that likely represent a mixture of air and small, partially or completely (i.e., dry) crystallized particles. It is uncertain whether this material was representative of the background volcanic aerosol prior to the local action of the jet streaks, but the properties of these stratospheric aerosols are in marked contrast to those observed earlier. Assuming that tropospheric mixing was responsible for the wider range of δ values measured on 4–5 August, our interpretation of the microphysical processes within the cloud layer is shown schematically in Fig. 8 in terms of mixed-phase cloud dynamics.

This analysis is based on the assumptions that sufficient time and volcanically-injected sulfurous gases were present to promote the formation of a sulfuric acid droplet cloud in the lower stratosphere during its transport to the local area, and that this material was rather abruptly mixed with tropospheric air within tropopause folds. According to Shapiro (1980), tropopause folds represent "mixing regions whose chemical characteristics lie somewhere between those of the troposphere and the stratosphere." The subsequent accelerated aerosol growth processes were dominated by the increased availability of both water vapor and ammonia gas that interacted with the acid droplets. Since a majority of the δ values in Fig. 8 fall within the 0.1–0.2 range that is in reasonable agreement with laboratory studies of partially crystallized sulfuric acid droplets (Sassen et al. 1989b), ammonia gas was apparently more important in terms of the depolarizing properties of the cloud particles. Acid droplets that do not become ammonia saturated will display near-zero δ values that increase slowly with increasing R due to multiple scattering (note the dashed line at the bottom of Fig. 8 showing an approximate R-versus-δ relationship similar to that of Kobayashi et al. 1987). Only a few of the data points fall within this regime for significant scattering ratios, and these occurred at ~2245 5 August near the cloud peak. However, because of the shortness of the data record on this occasion it can-

TABLE 1. Mean and peak cloud properties derived from averages of all lidar data collected during each observation period (note total numbers of useable lidar shots), except for the numbers in parentheses, which represent the maximum 10-shot average values. The cloud is defined by $R \geq 1.2$. Peak values are 75 m vertical averages.

				Peak values			
Period (UTC)	No. shots	Height (km)	τ_c[1]	Height (km)	R	β_c 10^{-3} (km sr)$^{-1}$	δ
4 August (0311–0500)	101	14.1–15.8	0.012 (0.020)	14.5	5.2 (8.8)	0.52 (0.95)	0.14 (0.16)
5 August (0218–0404)	137	14.1–16.0	0.013 (0.017)	15.1	6.5 (8.0)	0.62 (0.80)	0.16 (0.18)
5 August (2240–2247)	12	14.7–16.1	0.009	15.6	6.7	0.60	0.02
7 August (0243–0257)	25	~14.3–16.1	0.002	15.0	1.5	0.06	0.06

[1] Cloud optical thickness estimates are based on $k = 0.04$ and a multiple scattering correction factor of $\eta = 0.9$ (see Sassen et al. 1989a).

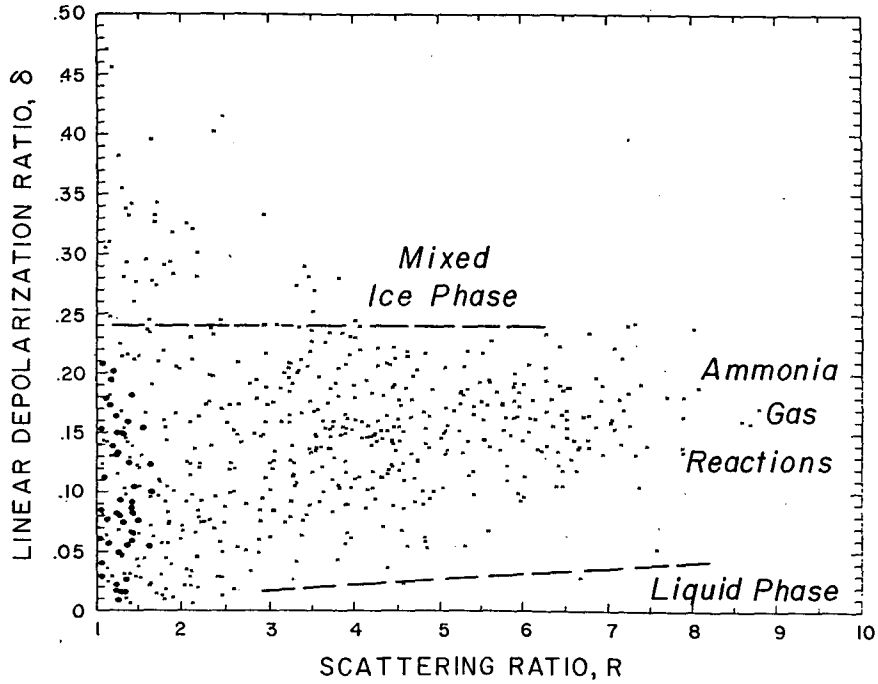

FIG. 8. Scatter plot of all 75 m vertically averaged δ values plotted against the scattering ratio. × and ● symbols are for all cloud data collected on 4–5 August and the weaker aerosol data for 7 August, respectively. The domains delineated by the dashed lines represent our appraisal of the indicated cloud microphysical content.

not be determined if this behavior was temporarily significant.

In contrast, $\delta > 0.25$ are mainly confined to the coldest cloud regions, particularly on 4 August, and range to a ~0.45 value appropriate for ice cloud scattering. The upper dashed line in Fig. 8 represents our appraisal of an approximate boundary between the δ values for crystallized acid droplets, and a mixture of droplets and ice crystals.

4. Conclusions

It is somewhat fortuitous that the aerosols were observed at Salt Lake City during early August 1989. Because the station was located to the north of the jet axis in the upper troposphere and there was a lack of significant cloud cover during this period, it was possible to collect a four-day sequence of sunset lidar measurements. (Cloudy skies with considerable midtropospheric moisture are common during August, as a result of the summer monsoon over the Great Basin region.) Jet streaks embedded within the synoptic-scale flow seem to have been responsible for making the aerosol layer more visible by subjecting the aerosols to large variations in altitude, temperature, and moisture. It is probable that the cloud was rapidly evolving overhead, and had it not been for the aerosol subduction causing considerably more favorable growth conditions, the event may have gone unnoticed and unstudied. In addition, the passage over SLC of relatively fresh volcanic materials from Central America would normally be uncommon during summer. Aerosols injected into the subtropical easterly flow that is typical during summer over Central America are likely to remain in the subtropical belt. In this instance, the presence of an upper troposphere/lower stratosphere trough to the east of Hawaii during the period 28–30 July appears to have allowed this fairly unusual exchange between the subtropics and midlatitudes.

On the basis of trajectory analyses, we have concluded that the 19 July 1989 eruption of the Guatemalan volcanic dome, Santiaguito, was the source of the aerosols observed 2–3 weeks later over the central Rocky Mountain region. We note that a brilliant red sunset on 5 August was reported by an observer in Golden, CO (39.8°N, 105.3°W), who also noted horizontal striations in the layer (SEAN Bulletin 1989). Although lidar systems in Hawaii and Virginia that normally monitor stratospheric aerosol content were unfortunately not in operation during early August, the Mauna Loa Observatory lidar detected slight enhancements in the scattering ratio ($R \leq 1.1$) with peaks at altitudes between 15.6 and 16.5 km from 16 August to 6 September (SEAN Bulletin 1989). These data confirm the presence of a new, shallow stratospheric eruption cloud. Although this material would likely have a relatively short residence time in the atmosphere due to the indicated low eruption cloud altitude, long-term lidar monitoring is needed to determine the eventual global impact of the Santiaguito eruption.

The variations in the cloud layer structure observed by the lidar are consistent with the striated patterns, noted visually, and imply the presence of wave-like clouds possibly induced by vertical wind shear in the jet streaks or by local orographic effects. The wave-like mesoscale circulations are associated with variations in the depolarizing properties of the cloud particles, implying a dynamic response in cloud composition. The majority of the δ values are consistent with laboratory measurements of partially crystallized sulfuric acid droplets caused by ammonia gas absorption (Sassen et al. 1989b). Only a few data points indicate homogeneous (i.e., not ammonia-saturated) droplets. Evidence for strong ice crystal depolarization was found at the coldest cloud temperatures encountered in association with relatively weak backscattering, which is contrary to the R-versus-δ relationship previously associated with stratospheric ice clouds. For example, scattering ratios in polar stratospheric clouds increased significantly as the environmental frost point was attained and ice clouds formed (Poole et al. 1990). In our case, it appears that ice crystal growth, in competing for the scarce water vapor supply, caused an overall reduction in ruby laser backscattering as the coexisting droplets began evaporating. The microphysical consequences of these rather exotic mixed-phase processes are difficult to comprehend without detailed modeling studies, but ambient temperature, along with the saturated solution droplet volume (possibly affected by droplet coalescence), may have controlled the ice nucleation process in the environment dominated by relatively slight vertical motions and turbulent mixing.

In conclusion, this relatively minor volcanic episode has provided an opportunity to study the details of the processes involved in the fate of all volcanically-injected stratospheric clouds—latitudinal dispersion and tropospheric removal. Tropopause folds that develop in midlatitude storms are responsible for the exchange of atmospheric trace gases such as ozone (Buzzi et al. 1985) and dynamical properties such as potential vorticity (Danielsen et al. 1987). The data given here also indicate that tropopause folding acts as an effective sink for lower stratospheric aerosol clouds of volcanic origin, as suggested earlier by Post (1986). Under these conditions, ammonia gas-acid droplet reactions appear to play a major role in cloud particle chemistry in the upper troposphere. Similar acid droplet neutralization processes that occur in the lower troposphere generate cloud condensation nuclei (CCN). The impulsive production of CCN across the variable boundary of the tropopause should, to some extent, affect the properties of upper tropospheric cirrus clouds, perhaps providing an additional mechanism for climatic perturbations following major volcanic eruptions. In this connection, we note that recent cirrus modeling studies (Sassen and Dodd 1989) indicate that fundamental cirrus cloud growth processes appear to be quite sensitive to the CCN spectrum.

Acknowledgments. The research has been supported by NSF Grants ATM-8513975 and ATM-8715360. We would like to thank H. Zhao for his contributions in lidar data processing.

REFERENCES

Ardanuy, P. E., and H. L. Kyle, 1986: Observed perturbations of the earth's radiation budget: A response to the El Chichón stratospheric aerosol layer? *J. Climate Appl. Meteor.*, **25,** 505–516.

Buzzi, A., G. Giovanelli, T. Nanni and M. Tagliazucca, 1985: Case study of stratospheric ozone descent to the lower troposphere during ALPEX. *Beitr. Phys. Atmos.*, **58,** 399–406.

Crum, F. X., and D. E. Stevens, 1988: A case study of atmospheric blocking using isentropic analysis. *Mon. Wea. Rev.*, **116,** 223–241.

Danielsen, E. F., R. S. Hipskind, S. E. Gaines, G. W. Sachse, G. L. Gregory and G. F. Hill, 1987: Three-dimensional analysis of potential vorticity associated with tropopause folds and observed variations of ozone and carbon dioxide. *J. Geophys. Res.*, **92,** 2103–2111.

Hofmann, D. J., and J. M. Rosen, 1983: Sulfuric acid droplet formation and growth in the stratosphere after the 1982 eruption of El Chichón. *Science,* **222,** 325–327.

Horel, J. D., L. R. Staley and T. W. Baker, 1988: The University of Utah Interactive Dynamics Program—One approach to interactive access and storage of meteorological data. *Bull. Amer. Meteor. Soc.*, **69,** 1321–1327.

Keyser, D., and M. A. Shapiro, 1986: A review of the structure and dynamics of upper level frontal zones. *Mon. Wea. Rev.*, **114,** 452–499.

Kobayashi, A., S. Hayashida, Y. Iwasaka, M. Yamoto and A. Ono, 1987: Consideration of depolarization ratio measurements by lidar—in relation to chemical composition of aerosol particles. *J. Meteor. Soc. Japan,* **65,** 303–307.

McCormick, M. P., and T. J. Swissler, 1983: Stratospheric aerosol mass and latitudinal distribution of the El Chichón eruption cloud for October 1982. *Geophys. Res. Lett.*, **10,** 877–880.

——, ——, W. P. Chu and W. H. Fuller, Jr., 1978: Post-volcanic stratospheric aerosol decay as measured by lidar. *J. Atmos. Sci.*, **35,** 1296–1303.

Poole, L. R., G. S. Kent, M. P. McCormick, W. H. Hunt, M. T. Osborn, S. Schaffner and M. C. Pitts, 1990: Dual-polarization lidar observations of polar stratospheric clouds. *Geophys. Res. Lett.*, **17,** 389–392.

Post, M. J., 1986: Atmospheric purging of El Chichón debris. *J. Geophys. Res.*, **91,** 5222–5228.

Rampino, M. R., and S. Self, 1984: Sulfur-rich volcanic eruptions and stratospheric aerosols. *Nature,* **310,** 677–679.

Russell, P. B., and R. D. Hake, 1977: The post-Fuego stratospheric aerosol: Lidar measurements, with radiative and thermal implications. *J. Atmos. Sci.*, **34,** 163–177.

Sassen, K., and G. C. Dodd, 1989: Haze particle nucleation simulations in cirrus, and applications for numerical and lidar studies. *J. Atmos. Sci.*, **46,** 3005–3014.

——, M. Griffin and G. C. Dodd, 1989a: Optical scattering and microphysical properties of subvisual cirrus clouds, and climatic implications. *J. Appl. Meteor.*, **28,** 91–98.

——, H. Zhao and G.-K. Yu, 1989b: Backscatter laser depolarization studies of simulated stratospheric aerosols: Crystallized sulfuric acid droplets. *Appl. Opt.*, **28,** 3024–3029.

SEAN Bulletin, 1989: Scientific Event Alert Network of the Smithsonian Institution. Vol. 15 (8), 18–21. [Available from the A.G.U.]

Self, S., M. R. Rampino and J. J. Barbera, 1981: The possible effects of large 19th and 20th century volcanic eruptions on zonal and hemispheric surface temperatures. *J. Volcano. Geotherm. Res.*, **11,** 41–60.

Shapiro, M. A., 1980: Turbulent mixing within tropopause folds as a mechanism for the exchange of chemical constituents between the stratosphere and troposphere. *J. Atmos. Sci.*, **37,** 994–1004.